Chemical Engineering Journal 136 (2008) 337–348

Chemical Engineering Journal

www.elsevier.com/locate/cej

Large eddy simulation of a bubble column using dynamic sub-grid scale model

M.T. Dhotre *, B. Niceno, B.L. Smith

Thermal-Hydraulics Laboratory, Nuclear Energy and Safety Department, Paul Scherrer Institute, CH-5232 Villigen-PSI, Switzerland

Received 18 September 2006; received in revised form 30 March 2007; accepted 11 April 2007

Abstract

Euler–Euler simulations of the gas–liquid flow in a square cross-sectioned bubble column with LES (two sub-grid scale models) and the k–ε model are presented. The sub-grid scale modeling is based on the Smagorinsky kernel in both its original form and the dynamic procedure of Germano. The attempt has been made to assess the performance of these two sub-grid scale models. The Smagorinsky model with model constant $C_s = 0.12$ performs quite well, and gives results almost identical to those given by the dynamic procedure of Germano. The SGS models are modified to account for bubble induced turbulence (Sato model) and it is observed that it does not change the results much. Predictions are also compared with the available experimental data. All the non-drag forces (turbulent dispersion force (only for RANS), virtual mass force, lift force) and drag force were incorporated in the model. An extended k–ε turbulence model has been used with extra source terms introduced to account for the interaction between the bubbles and the liquid. Though both LES models showed agreement in predictions, the Germano model still can be used to have estimates of C_s value which are not known a priori. Moreover, if objective is to understand the steady and time averaged features, RANS can also perform well.
© 2007 Elsevier B.V. All rights reserved.

Keywords: LES; RANS; Bubble column; Bubbly flow; Computational fluid dynamics

1. Introduction

Bubbly flows are encountered in several applications of industrial interest and different engineering areas, e.g. nuclear plants in nuclear engineering, bioreactors in chemical engineering separators, in oil and gas engineering. In nuclear power plants, bubbly flows are relevant for various design and safety issues. In particular, they can be found in the pressure suppression pool of evolutionary boiling water reactors (BWR). In passive cooling systems of such reactors, decay heat removal may be achieved by venting steam (mixed with non-condensable gases) into the suppression pool to reduce the pressure in the reactor system. There is the need to study in detail the complex 3D phenomena which will occur in these containment volumes (Smith [1]). In order to understand the phenomena, advanced modeling of the key phenomena is carried out at Paul Scherrer Institute (PSI) in the context of the NURESIM project (Cacuci et al. [2]). In view of this, an attempt has been made in the present work to understand the bubbly flows in simpler configuration, i.e. in a bubble column wherein gas is sparged at the bottom of the column, and rises through it in the form of bubbles. The resulting flow is characterized by many distinct flow structures of various length scales (from tiny vortices shed by an individual bubble to macroscopic circulation covering the whole column). The regime considered in present work is representative of the bubbly flows observed in chemical as well as nuclear industry.

During the last decade CFD as a research tool has opened the possibility to perform detailed study of two phase flow pattern in bubble columns. Various approaches have been suggested for solving the same fundamental flow problem and modeling may be attempted at various level of sophistication (for example, Delnoij et al. [3] using Eulerian–Lagrangian framework; Borchers et al. [4] using Eulerian Eulerian framework). Excellent account of the subject can be found in reviews of Jakobsen et al. [5], Joshi [6], Sokolichin et al. [7], Rafique et al. [8] and Mudde [9]. The turbulence of the continuous phase was incorporated through different models like the k–ε model (e.g. Pfleger et al. [10], Ekambara et al. [11]), k–ω model (e.g. Bech [12]), Reynolds Stress Model (e.g. Glover Cartland

* Corresponding author. Tel.: +41 56 310 2707; fax: +41 56 310 4481.
E-mail address: mahesh.dhotre@psi.ch (M.T. Dhotre).

1385-8947/$ – see front matter © 2007 Elsevier B.V. All rights reserved.
doi:10.1016/j.cej.2007.04.016

Nomenclature

BIV	bubble induced viscosity
CFD	computational fluid dynamics
C_μ	model constant in the k–ε model (–)
$C_{\mu,\mathrm{BI}}$	model constant for bubble induced turbulence (–)
$C_{\varepsilon 1}$, $C_{\varepsilon 2}$	constant in turbulence models (–)
C_D	drag coefficient (–)
C_L	lift force coefficien (–)t
C_VM	virtual mass force coefficient (–)
C_TD	turbulent dispersion coefficient (–)
C_s	sub-grid scale model constant (–)
d_B	bubble diameter (m)
E_o	Eotvos number (–)
g	gravitational constant (m s^{-2})
G	production of turbulent kinetic energy (kg m^{-1} s^{-3})
I	unity tensor
k	turbulent kinetic energy (m^2 s^{-2})
P	pressure (N m^{-2})
M_D	drag force (N m^{-3})
M_L	lift force (N m^{-3})
M_VM	virtual mass force (N m^{-3})
M_F	total interfacial force (N m^{-3})
u	axial component of velocity (m s^{-1})
$\mathbf{u}'$	fluctuating or sub-grid scale (SGS) velocity (m s^{-1})
v	lateral component of velocity (m s^{-1})
V_G	superficial gas velocity (m s^{-1})

Subscripts

G	gas phase (–)
k	either phase
L	liquid phase

Greek symbols

ϵ	volume fraction (–)
Δ	filtering width (m)
Δ_i	grid spacing in radial direction (m)
Δ_j	grid spacing in lateral direction (m)
Δ_k	grid spacing in axial direction (m)
ε	turbulent kinetic energy dissipation rate (m^2 s^{-3})
μ_L	dynamic viscosity (kg m^{-1} s^{-1})
ν	molecular kinematic viscosity of liquid (m^2 s^{-1})
ν_t	turbulent kinematic viscosity of liquid (m^2 s^{-1})
ρ	density (kg m^{-3})
σ_k	model constant k–ε model (–)
σ_ε	model constant k–ε model (–)
τ	stress tensor (N/m^2)

and Generalis [13]) and large eddy simulation (e.g. Deen et al. [14] and Vanga Reddy et al. [15] for a bubble column, Milelli [16], Lakehal et al. [17] for bubble plumes). The LES approach has been identified as a better way to model the turbulence by amongst others, Jakobsen et al. [5]. In LES, the scales of motion in a turbulent flow are separated into large and small scales; only the large scales of motion are computed explicitly and the effect of the unresolved small scales is modeled using closure laws that invoke an eddy viscosity hypothesis for the sub-grid stress terms. Since it is believed that small scales are more universal than large scales, one can hope that simpler algebraic models can be used to model them. It also means that LES has higher chances to be successful in flows where main phenomena are dominated by the existence of large coherent structures or eddies. Bubble columns fall into this category. Further, the interest in adopting LES in the present context is to permit the bubbles to directly interact with eddies which have at least the same size but not with smaller ones. Hence, turbulent energy dissipation that may occur at the sub-grid scale level due to the superposition of the liquid fluctuations and those induced by the bubbles are dictated by the energy containing eddies; this combined effect requires therefore a sub-grid scale model. The rationale behind use of LES for bubbly flows derives from the expectation that the large scale motions (which carry most of the energy) would be primarily responsible for the macroscopic influence of the turbulence on the bubble motion, including dispersion, whereas small-scale turbulence would be less important affecting more the localized bubble oscillations [17].

When envisaging the potential of LES for simulating bubbly flows, one should clearly identify the scales at which LES might be used, since this implies level of details of the interface resolution/modeling. Simulations at the meso-scale, i.e. scales larger than the interface details (bubble sizes), imply an Euler–Euler description of the interaction between the phases, such as described in this work. However, if LES for multiphase flows is applied at scales smaller than the bubble sizes (micro-scales), explicit interface tracking procedure would be needed (Niceno et al. [18]). The use of LES to capture the turbulent interactions between bubbles and the energy-containing large eddies in the continuous phase seems a very promising line of approach, since the large eddies mainly responsible for the interactions with the bubbles are explicitly resolved, while the smaller scale motions of the liquid may be modeled using simple sub-grid-scale (SGS) closure models.

Previous published work in two-fluid model LES, Milelli et al. [19] used a combination of the Euler–Euler approach and a LES model for the turbulence of the liquid phase. They studied the motion of a bubble plume in a cylindrical tank. Deen et al. [14] used similar approach and simulated the hydrodynamics in the bubble column with a square cross-section. They compared predictions of k–ε model and LES and reported that the LES compares better with the experimental data. Lakehal et al. [17] studied turbulent bubbly shear flows in a vertical square channel of which the inlet was separated into two equal halves by a splitter plate. An air–water mixture with different flow rates was introduced on either side of the splitter plate. More recently Vanga Reddy et al. [15] carried out LES using Smagorinsky model for rectangular column and compared predictions with transient computations performed with mixing length and k–ε model. They found that all three models produce similar results.

However, they carried out the simulation for a two-dimensional column which featured a large aspect ratio of the cross-section and the conclusions cannot be generalized for three-dimensional geometries.

In view of this, it was thought desirable to carry out large eddy simulation in three-dimensional square cross-sectional bubble columns. In the present work, we have followed the work of Deen et al. [14] and made an attempt to assess the performance of two sub-grid scale models, Smagorinsky [20] and Dynamic model of Germano et al. [21]. The predictions using LES (two sub-grid scale models) and k–ε model have been compared with the experimental data.

2. Mathematical modeling

The equations of motion for phase k in an Eulerian–Eulerian simulation are generally expressed as follows (Drew [23]):

$$\frac{\partial}{\partial t}(\rho_k \epsilon_k) + \nabla \cdot (\epsilon_k \rho_k \mathbf{u}_k) = 0, \tag{1}$$

$$\frac{\partial}{\partial t}(\epsilon_k \rho_k \mathbf{u}_k) + \nabla \cdot (\epsilon_k \rho_k \mathbf{u}_k \mathbf{u}_k) = -\nabla \cdot (\epsilon_k \tau_k) - \epsilon_k \nabla p + \epsilon_k \rho_k g + \mathbf{M}_{\mathrm{F},k} \tag{2}$$

The terms on the right-hand side of Eq. (2) are, respectively, representing the stress, the pressure gradient, gravity and the momentum exchange between the phases due to interface forces. The stress term of phase k may be described as follows:

$$\tau_k = -\mu_{\mathrm{eff}} \left(\nabla \mathbf{u}_k + (\nabla \mathbf{u}_k)^{\mathrm{T}} - \frac{2}{3} I (\nabla \cdot \mathbf{u}_k) \right) \tag{3}$$

where μ_{eff} is the effective viscosity which results from modeling the turbulent transport not resolved by computation. As proposed by Sato and Sekoguchi [24] the turbulent stress in the liquid phase of bubbly flow can be subdivided into two components, one due to the inherent, i.e. shear-induced, turbulence which is independent of the relative motion of bubbles and liquid, and the other due to the additional turbulence caused by bubble agitation, i.e. bubble-induced turbulence. The present formulation assumes that the effective viscosity of the liquid phase is composed of three contributions; the molecular viscosity, the turbulent eddy viscosity and an extra term to model the bubble induced turbulence

$$\mu_{\mathrm{eff}} = \mu_{\mathrm{L,L}} + \mu_{\mathrm{T,L}} + \mu_{\mathrm{BI,L}} \tag{4}$$

The model proposed by Sato et al. [25] has been used to take account of the turbulence induced by the movement of the bubbles. The expression used was as follows:

$$\mu_{\mathrm{BI,L}} = \rho_{\mathrm{L}} C_{\mu,\mathrm{BI}} \epsilon_{\mathrm{G}} d_{\mathrm{B}} |\mathbf{u}_{\mathrm{G}} - \mathbf{u}_{\mathrm{L}}| \tag{5}$$

with a model constant $C_{\mu,\mathrm{BI}}$ which is equal to 0.6. We use two approaches to calculate the turbulent eddy viscosity, $\mu_{\mathrm{T,L}}$: LES and the k–ε model.

2.1. Large eddy simulation

The velocities in Eqs. (1) and (2) are defined as follows:

$$\mathbf{u}_k = \tilde{\mathbf{u}}_k - \mathbf{u}'_k \tag{6}$$

Here, $\mathbf{u}_k$ is the part of the velocity for phase k that will be resolved in the numerical simulations, $\tilde{\mathbf{u}}_k$ the instantaneous velocity and $\mathbf{u}'_k$ is the unresolved part of the numerical simulations. When filtering operation (Leonard [26]), is used to obtain Eqs. (1) and (2), these terms are, respectively, the grid scale (resolved) and the sub-grid scale (unresolved) velocities. Hereafter, when speaking about velocities, we refer to $\mathbf{u}_k$, unless mentioned otherwise. We need a sub-grid model to model the unresolved turbulent scales. The key element in LES is the sub-grid scale model, which determines the effect of the unresolved scales of motion on the resolved scales. In the present study we have used two models. (a) The simple model of Smagorinsky [20] and (b) the dynamic model of Germano et al. [21].

Smagorinsky [20] used following expression to calculate the turbulent viscosity $\mu_{\mathrm{T,L}}$ i.e. the SGS viscosity:

$$\mu_{\mathrm{T,L}} = \rho_{\mathrm{L}} (C_{\mathrm{s}} \Delta)^2 |S| \tag{7}$$

where C_{s} is a model constant and S is the characteristic filtered rate of strain tensor and $\Delta = (\Delta_i \Delta_j \Delta_k)^{1/3}$ is the filter width. The disadvantage of this model is that the constant C_{s} must be set, and it seems to be different for different flows. In the literature for single-phase flow, the constant is found to vary in the range from $C_{\mathrm{s}} = 0.065$ (Moin and Kim [27]) to $C_{\mathrm{s}} = 0.25$ (Jones and Wille [28]). We used value of C_{s} equal to 0.12 for the present work based on previous experience of Lakehal et al. [17] and Milelli et al. [19]. In view of the uncertainty in specifying the constant C_{s}, Germano et al. [21] proposed a dynamic sub-grid model in which the constant C_{s} is not arbitrarily chosen (or optimized), but where it is computed. The main idea behind this new concept consists in introducing a filter, $\widehat{\Delta}$ with larger width than the original one, i.e. $\widehat{\Delta} > \Delta$. This filter is applied to the filtered Navier–Stokes equations (the NS equations are filtered twice), yielding the value of C_{s} derived from:

$$C_{\mathrm{s}} = -\frac{1}{2} \frac{L_{ij} M_{ij}}{M_{ij} M_{ij}} \tag{8}$$

where

$$L_{ij} = \widehat{\overline{u_i u_j}} - \widehat{\bar{u}}_i \widehat{\bar{u}}_j$$

and

$$M_{ij} = \left[\widehat{\Delta}^2 |\widehat{\bar{S}}| \widehat{\bar{S}}_{ij} - \widehat{\Delta}^2 \widehat{|\bar{S}| \bar{S}_{ij}} \right]$$

and the hat indicates that a second filter, usually called the test filter, which is twice the mesh size in the present study, has been applied to the velocity fields. This is standard procedure and details can be found elsewhere (Germano et al. [21], Lilly [29]).

2.2. Standard k–ε model

The interpretation of the terms $\mathbf{u}_k$ and $\mathbf{u}'_k$ in Eq. (2) changes for the RANS approach to turbulence modeling. When Eqs. (1)

and (2) are obtained through time averaging, then $\mathbf{u}_k$ and $\mathbf{u}'_k$ represent the mean velocity and the fluctuating velocity. When either time averaging or filtering is used, unclosed terms occur in the stress term (Eq. (3)) and in the interface forces, and must be modeled.

When k–ε model is used, the turbulent viscosity is formulated as follows:

$$\mu_{T,L} = C_\mu \rho_L \frac{k^2}{\varepsilon} \tag{9}$$

with the turbulent kinetic energy k and the energy dissipation rate, ε are calculated from their conservation equations. The governing equations for the turbulent kinetic energy k and turbulent dissipation ε are:

$$\frac{\partial}{\partial t}(\epsilon_L \rho_L k) + \nabla \cdot (\epsilon_L \rho_L \mathbf{u}_L k) - \nabla \cdot \left(\epsilon_L \frac{\mu_{T,L}}{\sigma_L} \nabla k\right) + \epsilon_L (G - \rho_L \varepsilon) + \mathrm{ST}_k \tag{10}$$

$$\frac{\partial(\epsilon_L \rho_L \varepsilon)}{\partial t} + \nabla \cdot (\epsilon_L \rho_L \mathbf{u}_L \varepsilon) = -\nabla \cdot \left(\epsilon_L \frac{\mu_{T,L}}{\sigma_\varepsilon} \nabla \varepsilon\right) + \epsilon_L \left(C_{\varepsilon 1} \frac{\varepsilon}{k} G - C_{\varepsilon 2} \rho_L \frac{\varepsilon^2}{k}\right) + \mathrm{ST}_\varepsilon \tag{11}$$

with standard model constants $C_{\varepsilon 1} = 1.44$, $C_{\varepsilon 2} = 1.92$, $C_\mu = 0.09$; $\sigma_k = 1$, $\sigma_\varepsilon = 1.3$. The term G in above equations is the production of turbulent kinetic energy and described by

$$G = \tau_L : \nabla \mathbf{u}_L \tag{12}$$

The model proposed by Simonin and Viollet [30] has been used to represent the migration of the gas bubbles through the liquid. The extra source terms are written for this model as:

$$\mathrm{ST}_k = C_{k2} C_f \rho_L \epsilon_G \epsilon_L k \tag{13}$$

$$\mathrm{ST}_\varepsilon = C_{\varepsilon 2} C_f \rho_L \epsilon_G \epsilon_L \varepsilon \tag{14}$$

here C_f is the interphase friction coefficient given by

$$C_f = \frac{3}{4} \frac{C_D}{d_B} |\mathbf{u}_G - \mathbf{u}_L|$$

The coefficients of this model are $C_{k2} = 0.75$, $C_{\varepsilon 2} = 0.6$.

2.3. Interfacial forces

The momentum exchange term $\mathbf{M}_{F,L}$ in Eq. (2) describing the interface forces is given as follows:

$$\mathbf{M}_{F,L} = -\mathbf{M}_{F,G} = \mathbf{M}_{D,L} + \mathbf{M}_{L,L} + \mathbf{M}_{VM,L} + \mathbf{M}_{TD,L}, \tag{15}$$

where the terms on the right hand side of Eq. (8) are forces due to the interphase drag, lift, virtual mass, and turbulence dispersion, respectively. All other components of the interfacial momentum transfer term besides the drag force are collectively referred to as the non-drag forces.

The origin of the drag force is due to the resistance experienced by a bubble moving in the liquid. Viscous stress creates skin drag and pressure distribution around the moving bubble creates form drag. The drag force per unit volume is written in the following form (Clift et al. [31]):

$$\mathbf{M}_{D,L} = \frac{3}{4} \epsilon_G \rho_L \frac{C_D}{d_B} |\mathbf{u}_G - \mathbf{u}_L| (\mathbf{u}_G - \mathbf{u}_L) \tag{16}$$

The drag coefficient C_D depends on the flow regime and the liquid properties. The Reynolds number covered in the present work falls under the inertial range and as per the visual experimental observation bubbles become distorted in this region. Ishii and Zuber [32] give the following expression for the drag coefficient C_D in the case of distorted bubbles:

$$C_D = \frac{2}{3} E_o^{1/2} \tag{17}$$

where E_o is the dimensionless Eötvös number ($E_o = g \Delta\rho d_B^2/\sigma$). In this work, a bubble size of 4.0 mm is used, giving $E_o = 2.2$ and $C_D = 1.0$. The bubble size is in correspondence with the observations of Deen et al. [22]. A sensitivity analysis for the value of C_D has been investigated in the present work.

A bubble traveling through a fluid in shearing motion will experience lift force transverse to the direction of motion. The effect of shearing motion in the liquid phase on the movement of the gas phase is modeled through the lift force as (Zun [33], Drew and Lahey [34]).

$$\mathbf{M}_{L,L} = \epsilon_G \rho_L C_L (\mathbf{u}_G - \mathbf{u}_L) \times \nabla \times \mathbf{u}_L \tag{18}$$

where C_L is a model constant which is set to 0.5.

The virtual mass force accounts for relative acceleration, the additional work performed by the bubbles in accelerating the liquid surrounding the bubble (Jakobsen et al. [5]). The acceleration of the liquid is taken into account through the virtual mass force, which is given by

$$\mathbf{M}_{VM,L} = \epsilon_G \rho_L C_{VM} \left(\frac{D\mathbf{u}_G}{Dt} - \frac{D\mathbf{u}_L}{Dt}\right) \tag{19}$$

where the virtual mass coefficient C_{VM} is generally shape dependent and is taken to be 0.5 for individual spherical bubbles. The D/Dt operators denote the substantial derivatives in the two phases. At the start of each run, initially the virtual mass force was deselected and this effect was taken into account by simply using an enhanced gas density (Smith [1]).

$$\rho'_G = \rho_G + C_{VM} \rho_L \tag{20}$$

in the acceleration term of the gas momentum Eq. (2).

It should be noted that the drag and lift forces depend on the actual relative velocity between the phases, but the Reynolds-averaged equations of motion for the liquid only provide information regarding the mean flow field. To account for the random influence of the turbulent eddies; the concept of a turbulent dispersion force has been advanced. By analogy with molecular movement, the force is set proportional to the local bubble concentration gradient (or void fraction), with a diffusion coefficient derived from the turbulent kinetic energy. The force derived by Lopez de Bertodano [35] approximates a turbulent diffusion of the bubbles by the liquid eddies. It is formulated as:

$$\mathbf{M}_{TD,L} = C_{TD} \rho_L k \nabla \epsilon_G \tag{21}$$

where k is the liquid turbulent kinetic energy per unit of mass. The turbulent dispersion coefficient C_{TD} of 0.2 was found to give the best results in prediction of axial liquid and gas velocity in the present work. It should be noted that the turbulence dispersion force was only used for k–ε model.

3. Method of solution

A commercial CFD package CFX, Version 4.3 was used to solve the equations of continuity and momentum. This package is a finite volume solver, using body-fitted grids. A schematic of the Deen et al. [22] experimental set-up is shown in Fig. 1. It consists of column with 0.15 m × 0.15 m cross-section and filled with distilled water up to the height of 0.45 m. A distributor plate containing 49 holes with diameter of 1 mm were placed in the middle of the column at the base. The boundary conditions were defined as follows. At the inlet the gas velocity was calculated using the superficial gas velocity and the area inlet, using the fact that total volumetric flow remains the same in the column at any level,

$$V_{G,in} = \frac{V_G A_C}{\epsilon_G A_{in}} \tag{22}$$

where V_G is the superficial gas velocity and A_c is the cross-sectional area of the column. The gas inlet area A_{in} (0.03 m × 0.03 m) was implemented in a central area of 3 × 3 grid cells for coarse grid and 6 × 6 grid cells for the fine grid. The first node near the wall has y^+ of 120 and 70 for coarse and fine grid, respectively. A superficial gas velocity of 4.9×10^{-3} m/s leads to a gas velocity at the inlet of 0.12 m/s for both the grid spacing. Along the walls, the no-slip boundary condition was adopted. For the k–ε model, wall functions were applied whereas in case of LES, this condition was imposed using the wall treatment of Werner and Wengle [36]. This approach was earlier successfully used by Lakehal et al. [17]. The top of the air layer is modeled as a pressure–constant boundary (relative $p = 0$). This condition was applied for both RANS and LES in order to fully capture the details of the free surface. For LES, two test simulations were carried out, with and without the free surface. Results from these two computations revealed that consideration of the deformation of the free surface does not substantially modify the solution, and a flat surface is a good approximation. In view of this, the flat surface approximation was adopted for further LES computations to economize on computing time. It was also observed that with and without extended flow domain, the RANS approach also showed insignificant change in predictions. However, the savings in terms of CPU times was not great, so the air blanket was retained for all computations carried out using RANS.

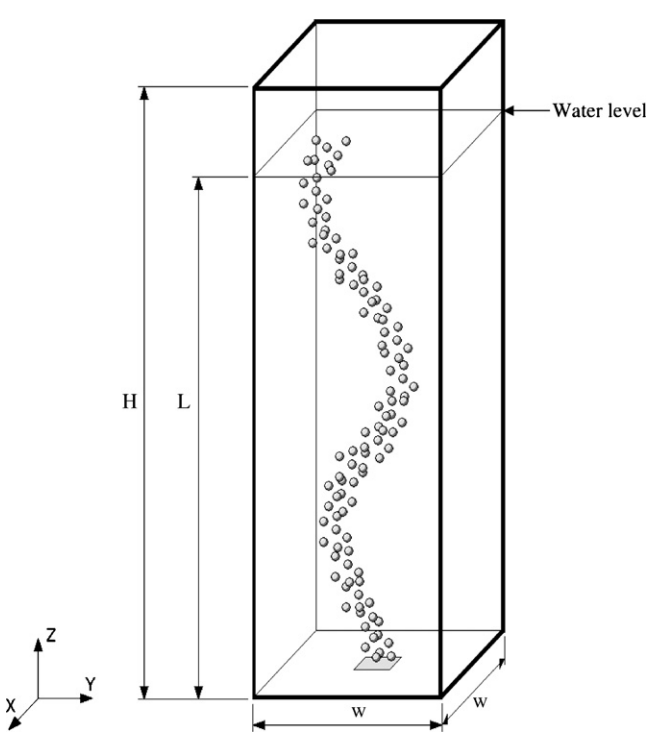

Fig. 1. Schematic of the numerical set-up for experiments of Deen et al. [22] ($W = 0.15$, $H = 0.5$, $L = 0.45$ m).

In all the simulations, a bounded, third-order-accurate QUICK scheme was used for the discretization of the advection term and a second-order; fully implicit backward differencing scheme was used for the time variable. All the simulations were carried out using the well-tested PSI beta version of the CFX 4.3 code (Smith and Milelli [37]) and appropriate user-defined subroutines. The following section discusses the grid requirement criterion for LES.

3.1. Grid requirement

In the present work, we couple the Euler–Euler approach for multiphase modeling with LES, and therefore have to consider the resolution requirements of both techniques in order to choose a satisfactory grid. As shown by Niceno et al. [18], a basic requirement imposed by the Euler–Euler approach is that the control volume size is large enough to encompass all the interface details. This was the intrinsic assumption in the derivation of the Euler–Euler model equations, and strictly has to be satisfied at the discrete level as well. In LES, the SGS model is often very simple and only drains energy from the resolved field. Therefore, our goal in LES is to resolve as much as possible, and to have as fine a grid as feasible for the available computer hardware. Since the Euler–Euler approach specifies the minimum control volume size, whereas for LES we are invariantly seeking as fine a grid as possible, the requirements from the numerical grid by LES may sometimes conflict with the requirements of the Euler–Euler approach. This is illustrated in Fig. 2(a and b), which sketches the turbulence spectra (Niceno et al. [18]).

For successful LES, we must have a filter width (Δ) in the inertial sub-range region, and all scales of motion larger than that (left of Δ in Fig. 2a and b), must be accurately resolved on the numerical grid. If, however, we have a bubble diameter (d_B) larger than Δ (Fig. 2a), it is obvious that they would induce some large-scale motions, but this is not properly accounted for by simulation, since we have no information on interface details and its influence on the resolved large-scale motions. If we use a model for bubble-induced turbulence, it would even drain the energy from the resolved field, further deteriorating the accuracy

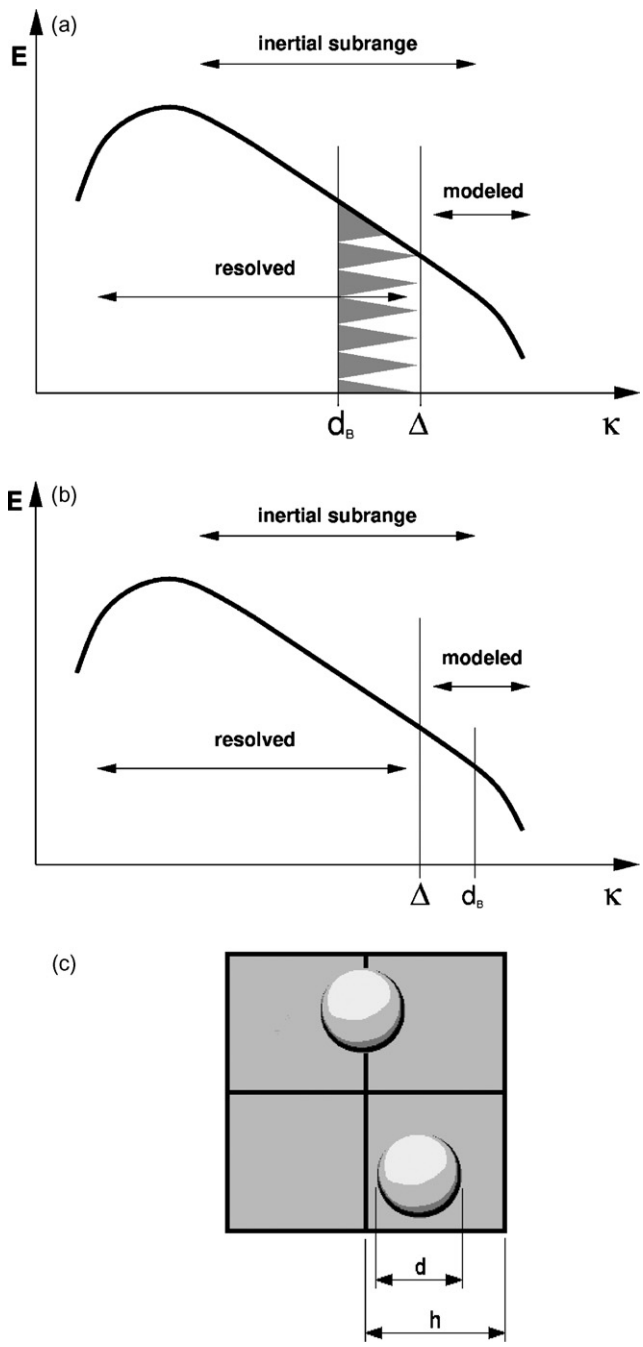

Fig. 2. (a) Spectra for condition when bubble size larger than filter width (Niceno et al. [18]), (b) spectra for condition when bubble size smaller than filter width (Niceno et al. [18]), (c) Milleli [16] condition.

of the resolved field. This is illustrated by the saw-like shading in Fig. 2a. This influence on the resolved part of the spectra is not acceptable for LES.

The situation which is safe for Euler–Euler–LES is shown in Fig. 2b, where d_B is smaller than Δ, and all bubble induced scales, which cannot be calculated with Euler–Euler–LES, fall into SGS part of the spectra. This is not just a conceptual consideration, as shown by Milelli [16], who made an a-posteriori analysis of the minimum ratio of the bubble and cell size for LES for bubble plumes and came up with the criterion: $h/d_B > 1.5$. The criterion states that cell size must be at least 50% larger than the bubble diameter for accurate LES. The situation is illustrated in Fig. 2c (Niceno et al. [18]).

In the present work, the bubble diameter was specified as 4 mm based on experimental observation. The flow is dominated by the energetic, large-scale structures in the core of the flow, with wall effects having a smaller impact on the overall flow field, so we used a uniform grid with 15 × 15 × 50 (coarse grid), 30 × 30 × 100 cells (fine grid). Since the dimensions of the domain are 15 cm × 15 cm × 50 cm, ratio h/d_B is 1.2 for the fine grid and 2.5 for the coarse grid. A simulation over 150 real-time seconds needs roughly 72 and 192 h for coarse and fine grid, respectively, on an AMD optron single-processor machine.

4. Results and discussion

The simulations of gas liquid flow in a bubble column have been carried out with two different approaches as described in the earlier section using CFX 4.3. The details of the cases simulated is given in Table 1. Deen et al. [14] carried out the LES using Smagorinsky model. In view of this, in the present study, the effect of interfacial forces for LES has not been reported to avoid repetition. Instead, new results with Germano model and sensitivity analysis for RANS have been provided in the following sections. Further, in case of RANS, attempt has been made to bring out effect of turbulent dispersion force on the predictions.

The simulations have been carried out using the time step between 0.005 and 0.01 s, depending upon the resolution. The time step was selected by applying the CFL-criterion, i.e. $\Delta t \leq \Delta z/|\mathbf{u}|$. No significant effect was observed by refining the time step. The simulations were run for 20 s before any flow statistics were collected. This allowed for all the initial dynamics of establishing the flow from zero velocity start condition to die out. Statistical data was collected over the period of next 130 s. A time history plot of the axial liquid velocity at one point ($z = 0.25$ m, $x = y = 0.075$ m) in the column is shown in Fig. 3 between 100 and 150 s. From this figure, it can be seen that, provided that drag, lift and virtual mass forces are taken into account, LES represents the transient behaviour observed in the experiments of Deen et al. [22] in terms of frequency and amplitude of the fluctuations. Both the time and velocity scales are fairly in agreement with the experimental data. It should be noted that both the sub-grid scale models capture the experimental observation reasonably well. In contrast, only large scale fluctuations which are small in magnitude are resolved in the k–ε

Table 1
Overview of models and grid spacing

Case	Δ_x, Δ_y Δ_z (mm)	Δt	Model	Forces
1	10.0	0.01	Ex-RANS[a], BIV	$\mathbf{M}_D$, $\mathbf{M}_L$, $\mathbf{M}_{VM}$, $\mathbf{M}_{TD}$
2	10.0	0.005	LES, Smagorinsky, BIV	$\mathbf{M}_D$, $\mathbf{M}_L$, $\mathbf{M}_{VM}$
3	10.0	0.005	LES, Germano, BIV	$\mathbf{M}_D$, $\mathbf{M}_L$, $\mathbf{M}_{VM}$
4	10.0	0.005	LES, Germano	$\mathbf{M}_D$, $\mathbf{M}_L$, $\mathbf{M}_{VM}$
5	6.0[b]	0.005	LES, Germano, BIV	$\mathbf{M}_D$, $\mathbf{M}_L$, $\mathbf{M}_{VM}$

[a] k–ε model with extra terms by Simonin and Viollet [30].
[b] Up to 450 mm in the z-direction.

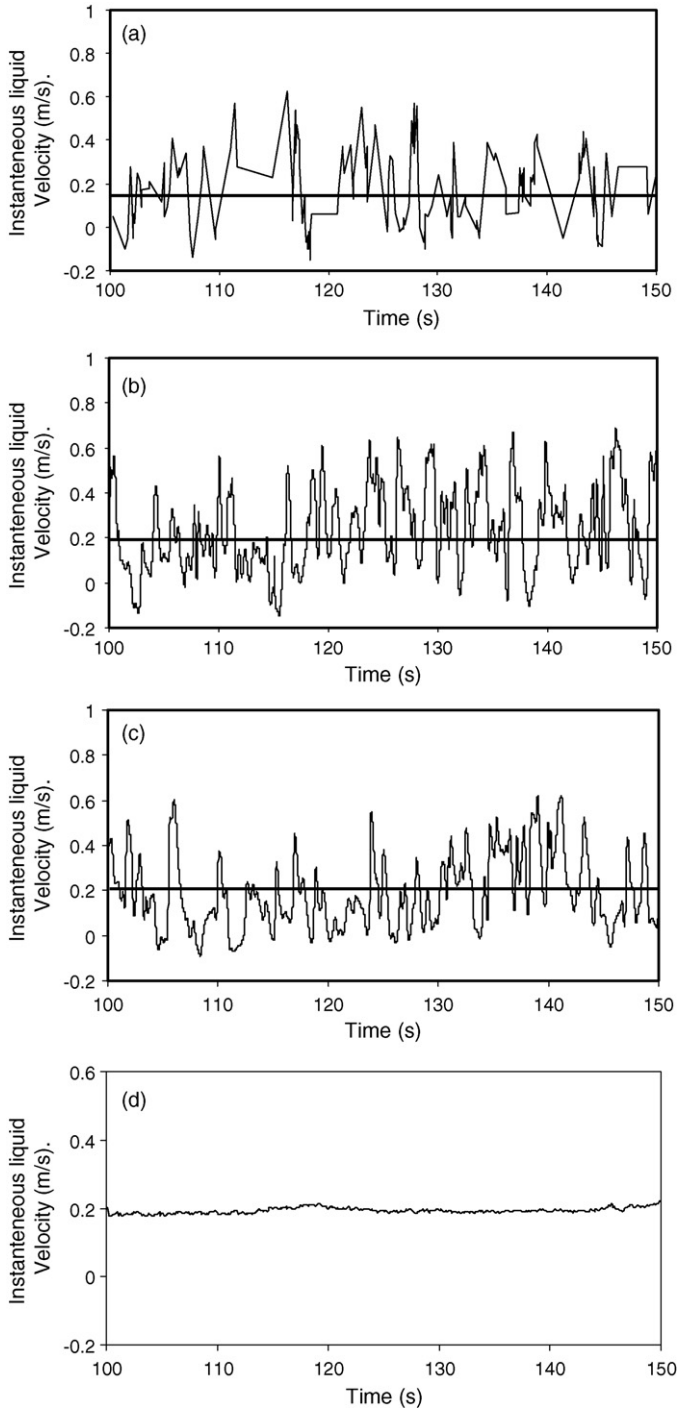

Fig. 3. Time history of the axial liquid velocity at the centerline of the column, at a height of 0.25 m. (a) LDA experiments, (b) Germano prediction, (c) Smagorinsky prediction (dark line: mean profile, faint line: fluctuating velocity profile), (d) RANS predictions.

model predictions. All the small-scale velocity fluctuations are contained in the turbulent kinetic energy k. It should be noted that RANS predictions agree reasonably well with the mean velocity predicted by all the models.

The energy spectrum obtained with data extracted from LES is shown in Fig. 4. The spectrum exhibits broad-range turbulence, with a slope changing between the single phase −5/3 and two-phase −10/3 power laws in the inertial sub-range. Previous experimental studies have actually attributed the more dissipative spectrum to the presence of the dispersed phase, this being responsible for eddy disintegration (Lance and Bataille [38]). The spectrum shown in Fig. 4 was taken at a one point ($z = 0.25$ m, $x = y = 0.075$ m) using the time series obtained from the LES simulation employing the Smagorinsky SGS model.

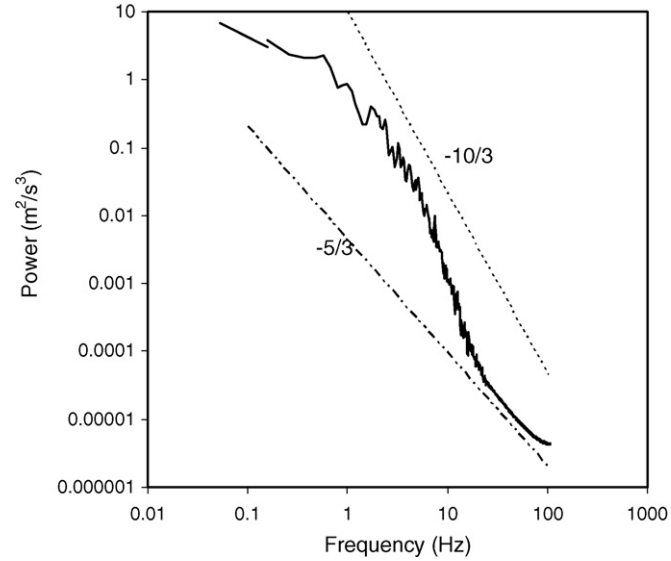

Fig. 4. Power spectra taken at a one point ($z = 0.25$ m, $x = y = 0.075$ m).

Deen et al. [14] examined the effect of interface forces and they have observed that plume spread can be captured when all the three forces are used in the model. They found that the lift force has significant role on plume spreading whereas the virtual mass force does not have significant impact on the predictions. Similar observations were made in the present study, but are not reported in detail here. In Figs. 5 and 6, snapshots of liquid velocity fields are displayed for all the three models at 40 and 150 s, respectively. Similar to the results shown in Fig. 3, the LES models resolve many more details of the flow. Large vortices can be observed along the side of the bubble plume. Note that the flow pattern changes with time. With RANS, the transient details are not resolved, but are implicitly contained in the turbulent kinetic energy. It is seen that a large stationary vortex is obtained next to the bubble plume.

For comparing the predictions with experimental data, the average velocities are calculated during the simulation, according to the following prescription:

$$\overline{u_{k,n}^2} = \frac{t_n - t_0 - \Delta t}{t_n - t_0} \cdot \overline{u_{k,n-1}^2} + \frac{\Delta t}{t_n - t_0} \cdot u_{k,n}^2 \tag{23}$$

where t_0 is the time from where gathering the statistics have been started, Δt the numerical time step and t_n is the current time.

The effect of the bubbles on turbulence in the continuous phase has been modeled using Sato's eddy viscosity model for bubble induced turbulence (Eq. (5)). In order to see its effect, simulations have been carried out with and without the model for the case of Germano model and is shown in Fig. 7. It can be seen from Fig. 7 which shows the prediction of axial liquid

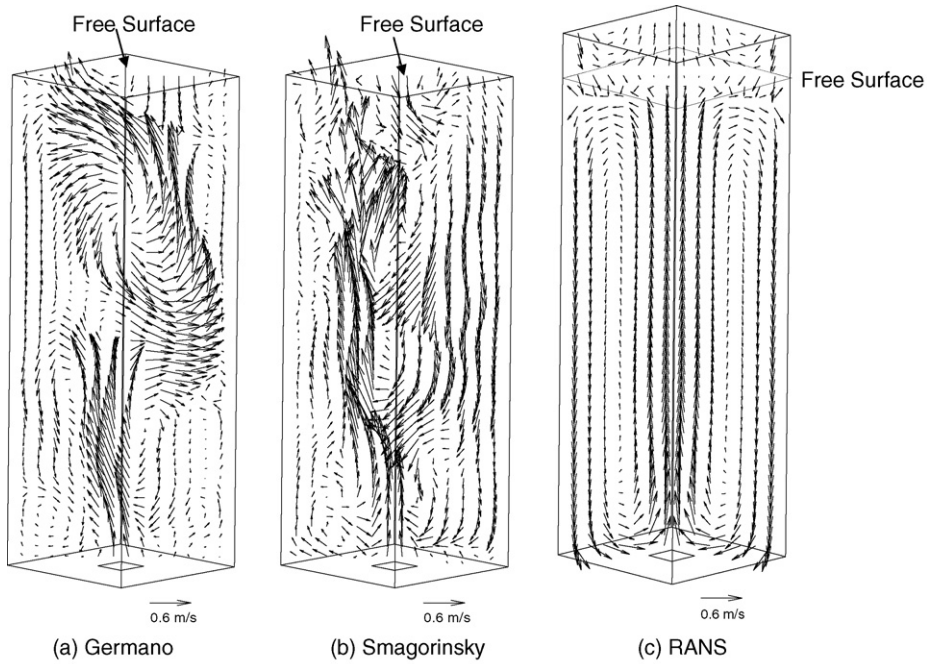

Fig. 5. Predicted instantaneous vector flow field for axial liquid velocity after 40 s for all three models.

velocity, that there is not significant change in the predictions with and without bubble induced turbulence model of the form proposed by Sato. This observation is in agreement with the results reported by Deen et al. [14] and Vanga Reddy et al. [15] who used CFX 4.3 and FLUENT for LES calculations, respectively. Fig. 7 also shows the comparison of coarse grid and fine grid predictions for the case of Germano model. It can be seen that the coarse grid predictions reasonably captures the experimental observation. The predictions with fine grid show good agreement with the experimental observations.

Figs. 8 and 9 shows quantitative comparison between the three turbulence models for the average mean velocity profiles of the liquid and the gas phase, respectively. It can be seen that all three models capture the experimental observations reasonably well. It can be observed that the axial gas velocity is over predicted by all the three models, best results being calculated by

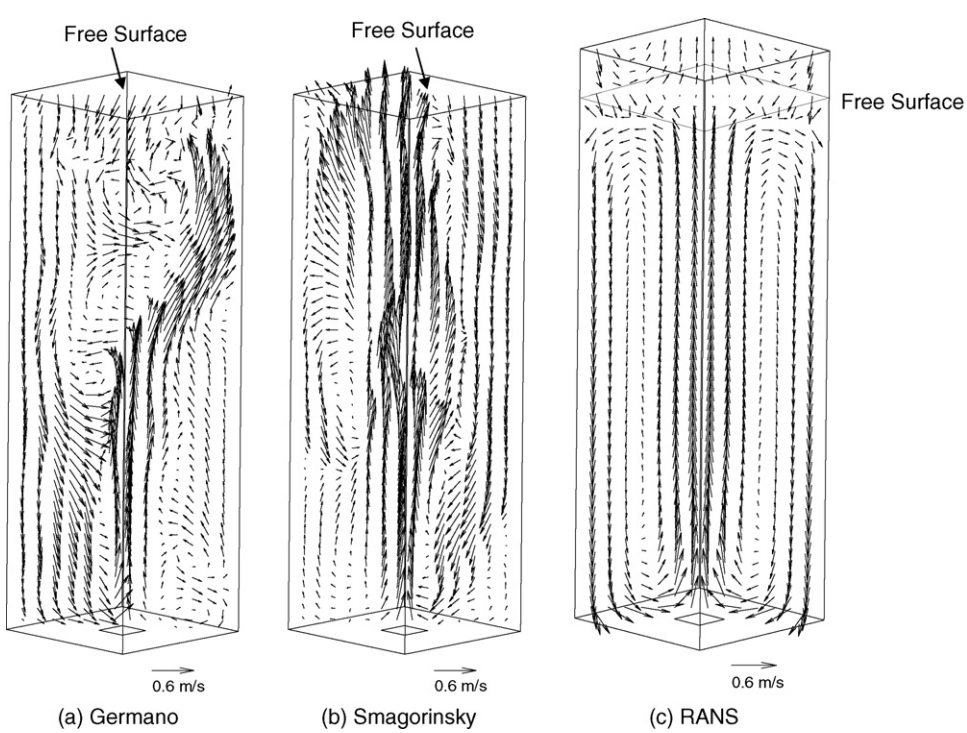

Fig. 6. Predicted instantaneous vector flow field for axial liquid velocity after 150 s, for all three models.

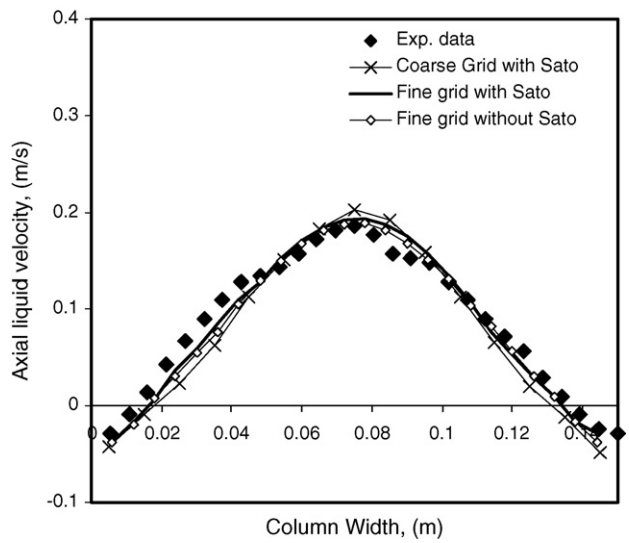

Fig. 7. Effect of bubble induced turbulence and grid sensitivity on prediction of axial liquid velocity distribution using SGS Germano model.

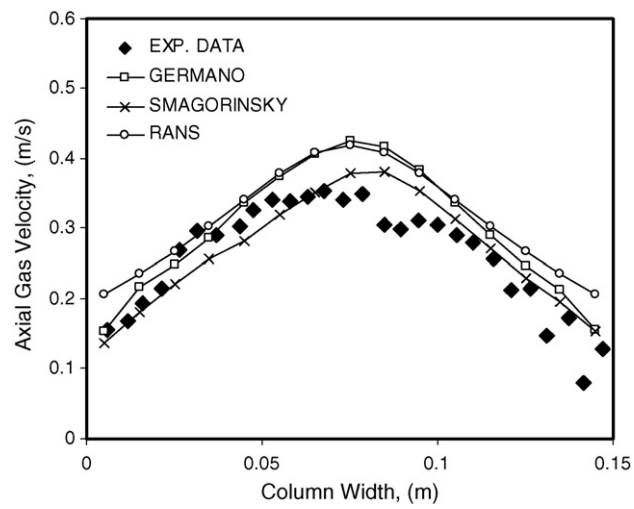

Fig. 9. Comparison of model predictions and experimental data for axial gas velocity at a height of 0.25 m, for three turbulence models.

the Smagorinsky model. An obvious explanation for the higher slip velocity predictions could be improper drag coefficient. In view of this, a sensitivity study has been carried out taking different drag coefficient (in the range of 0.85–1.1) which resulted in insignificant change in axial gas velocity. The reason for the over predictions of gas velocity is thus not clarified and should be subject of further investigations. Further, it should be noted that two sub-grid scale model predict the axial liquid and gas velocity more or less in identical way and that the k–ε model predictions are in agreement with the LES predictions. This is contrary to results of Deen et al. [14]. This may be attributed to the fact that Deen et al. [14] did not use lift force, virtual mass force and turbulent dispersion force in their calculation while using k–ε model. Fig. 10 shows the comparison of predictions with various contributions of forces. It can be observed that especially the inclusion of the turbulent dispersion force improves the results significantly. The consideration of turbulent dispersion in the simulation results in a further decrease of liquid velocity and flat profile. Reason for this more and more homogenous up-flow is a greater and more equal distribution of bubbles over a cross-section due to the dispersion. Further, we investigated the effect of the extra source terms in k and ε equations (Eqs. (13) and (14)) which are responsible for the bubble induced turbulence. It can be seen from Fig. 10 that when these terms are used along with all the forces, there is no significant change in the predictions of the mean velocities.

Figs. 11 and 12, show profiles of the axial and lateral fluctuations of the liquid velocity. In the k–ε model the velocity fluctuations are not resolved but contained in the turbulent kinetic energy, k. Assuming local isotropy of the turbulence, the

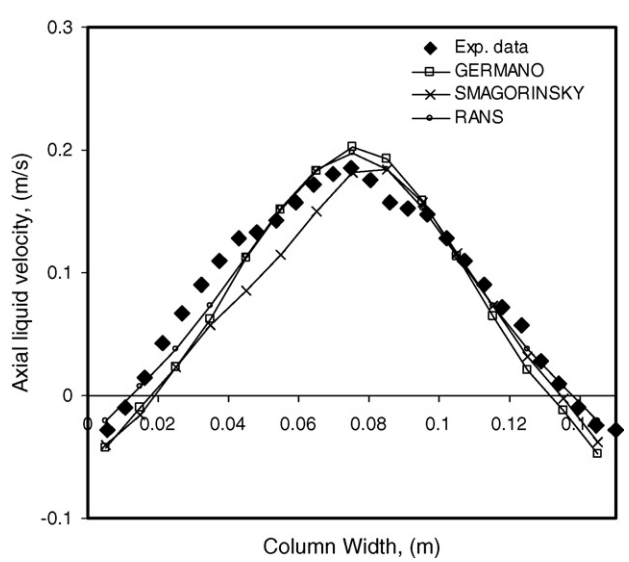

Fig. 8. Comparison of model predictions and experimental data for axial liquid velocity at a height of 0.25 m, for three turbulence models.

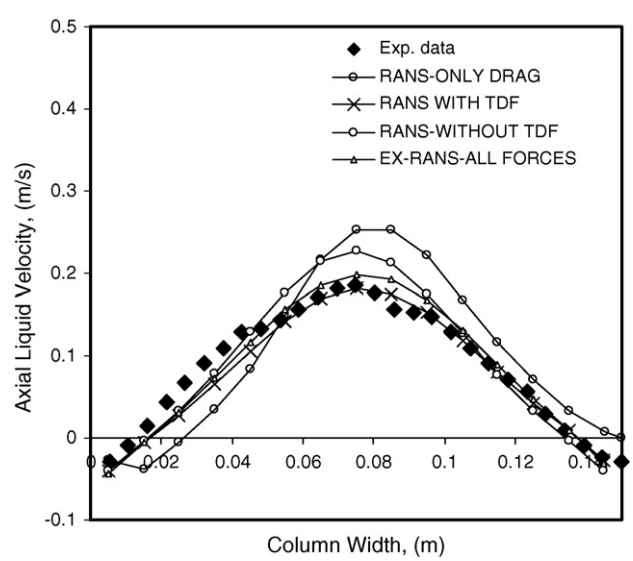

Fig. 10. Effect of forces on RANS predictions.

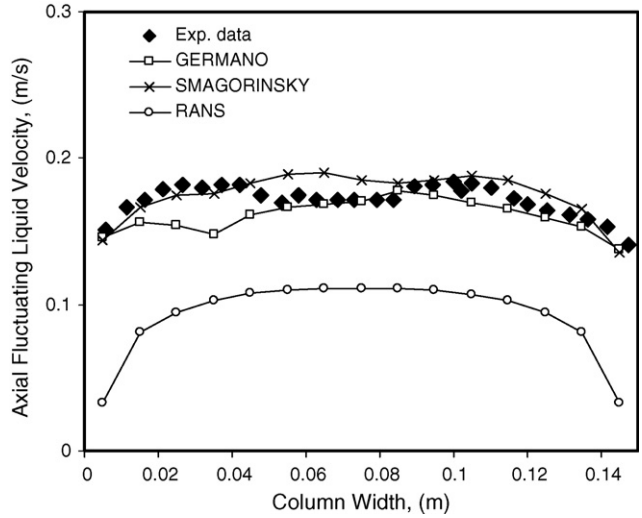

Fig. 11. Comparison of model predictions and experimental data for axial liquid velocity fluctuations at a height of 0.25 m, for three turbulence models.

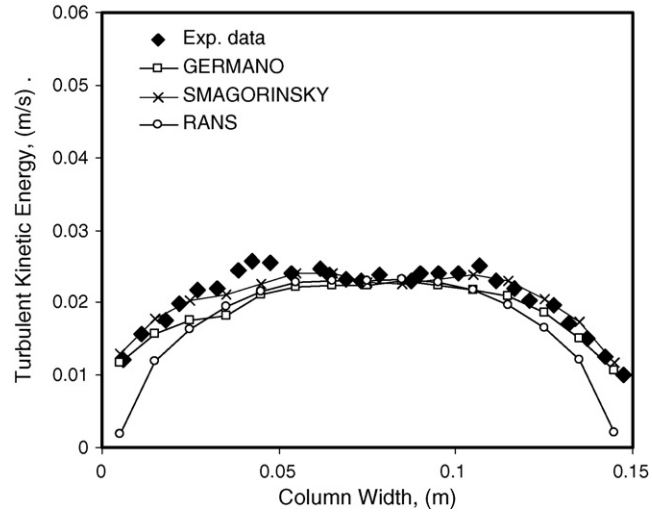

Fig. 13. Comparison of model predictions and experimental data for turbulent kinetic energy at a height of 0.25 m, for three turbulence models.

velocity fluctuations in each direction can be derived as follows:

$$\overline{u'^2_{\mathrm{L}}} = \overline{v'^2_{\mathrm{L}}} = \overline{w'^2_{\mathrm{L}}} = \frac{2}{3}k \tag{24}$$

In the RANS predictions, the axial velocity fluctuations are very low and lateral velocity fluctuations are too high. In the LES the velocity fluctuations in the three coordinate directions are calculated separately during the simulation. It can be seen from these experimental data that the assumption of isotropy is not valid, but both the sub-grid scale models for LES are able to perform much better in that respect. Both profiles show good agreement with the experimental data. Finally the predictive performance of all the models can be discussed within context of Fig. 13 which shows the comparison of the turbulent kinetic energy for all the three models. It can be seen that the simulations with the k–ε model and both sub-grid scale LES model capture the experimental distribution reasonably well. It can be however observed that the predictions with the k–ε model are poor near the wall. Further, refining the grid improved the results very little. The under-prediction of kinetic energy near the wall with the k–ε model can be attributed to several factors. First, the inappropriateness of standard wall functions, which are basically meant for single phase flow. Second, the turbulence is a multi-scale phenomenon, with extremely complex energy cascades in multiphase flows. Models like k–ε phenomenologically model turbulent kinetic energy production at large scales and its dissipation as small scales (Tennekes and Lumley [39]). By averaging the Navier–Stokes equations in time, we are inevitably losing the turbulent intensities of the large-scale structures near the wall.

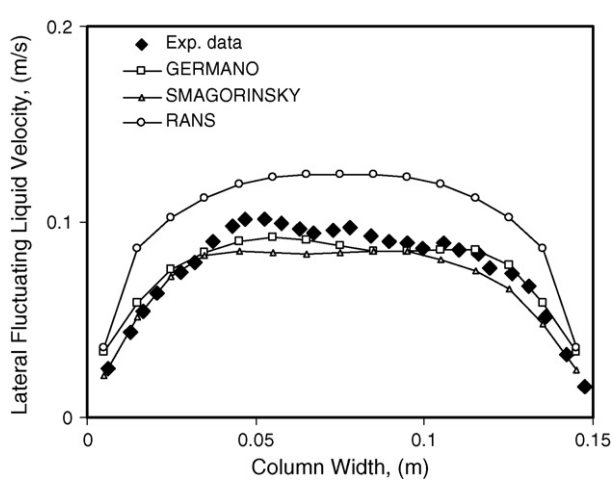

Fig. 12. Comparison of model predictions and experimental data for lateral liquid velocity fluctuations at a height of 0.25 m, for three turbulence models.

The LES results with two SGS models are almost identical and in accordance with the experimental data. Out of the two sub-grid scale model, the performance of the Germano model is not better than that of the Smagorinsky model. Since, it is generally believed that a dynamic model would give better performance for time and space developing flows (Germano et al. [21]), for flows dominated by near-wall effect, transitional flow, and if grid resolution is fine, this is not surprising. In those simulations the flow is under rapid change and a constant C_s in the Smagorinsky sub-grid scale model would not be expected to perform very well and account for the different, complicated flow features. This motivated us to check the local values of C_s, computed by the Germano model for this case. Fig. 14 shows the probability density function of the C_s over the entire column. It can be clearly seen that value of C_s equal to 0.12–0.13 has highest probability. It should be noted that the simulations carried out in the present study using Smagorinsky model uses the value of C_s equal to 0.12. This explains why the results are similar for both the SGS models. Further, sensitivity analysis of the constant C_s in Smagorinsky model has been carried out taking the two different values i.e. 0.09 and 0.15, which resulted in under and over prediction of centerline velocities by 30 and 25%, respectively. In view of this, one can conclude that the Germano model can give correct estimate of C_s value for the configuration/system under consideration and, in general, can

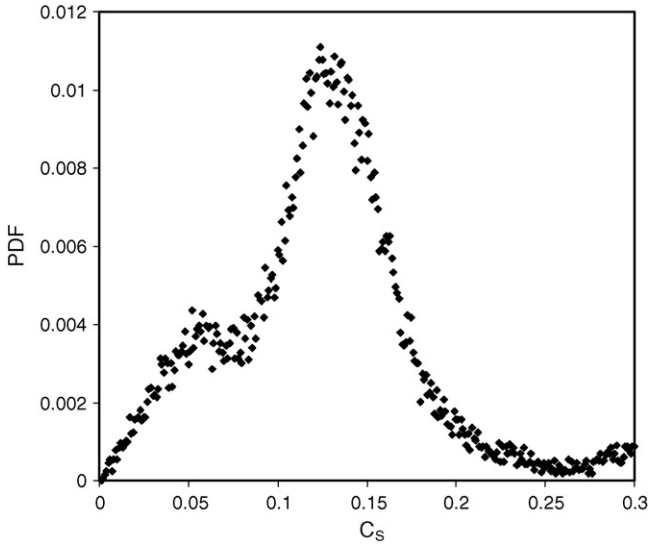

Fig. 14. Probability density function for computed constant C_s in Germano model over entire column.

be used for other systems where C_s is not known "a priori" from previous analysis.

5. Conclusion

The simulations have been carried out for the square cross-sectioned bubble column. Euler–Euler simulations of the gas–liquid flow in a bubble column using a LES (two sub-grid scale models) and k–ε model predictions has been compared with the experimental data from Deen et al. [22]. An extra contribution in the effective viscosity for the turbulence induced by bubbles was taken into account using the Sato model. The performance of two different sub-grid scale models, the Smagorinsky model and the Dynamic model of Germano, has been assessed. Modifying the SGS models to account for bubble induced turbulence did not change the results much. It was observed that the dynamic approach of Germano does not perform better than the Smagorinsky model for this configuration with C_s equal to 0.12. In fact, it is found that the averaged C_s values obtained with the Dynamic model converge towards $C_s = 0.12$. However, though Germano model predictions agree with Smagorinsky, still it can be used to have estimates of C_s value which are not known a priori. As for the k–ε model, it was found that with all the forces incorporated and using the extra source terms (Simonin and Viollet [30]) for turbulent kinetic energy and dissipation rate, the standard k–ε model gives reasonably good agreement with the mean experimental data except for the radial and axial distribution of the fluctuating liquid velocity and turbulent kinetic energy close to the wall.

Acknowledgements

The work reported in this paper was partly funded by the European Commission (6th Euratom Framework Programme 2002–2006) within the scope of the NURESIM project. The authors wish to thank Dr. Deen for his valuable help and suggestions in the analysis and also for sharing the experimental data. The authors are also grateful to their colleague Dr. Andreani for several technical inputs and suggestions during the preparation of the final manuscript.

References

[1] B.L. Smith, On the modelling of bubble plumes in a liquid pool, Appl. Math. Modell. 14 (1998) 67–76.
[2] D.G. Cacuci, J.M. Aragones, D. Bestion, P. Coddington, L. Dada, C. Chauliac, NURESIM: A European Platform for Nuclear Reactor simulation, in: FISA: Conference on EU Research and Training in Reactor Systems, Luxembourg, 2006.
[3] E. Delnoij, J.A.M. Kuipers, W.P.M. van Swaaij, A three dimensional CFD model for gas–liquid bubble columns, Chem. Eng. Sci. 54 (1999) 2217.
[4] O. Borchers, C. Busch, A. Sokolochin, G. Eigenberger, Applicability of standard k–ε turbulence model to the dynamic simulation of bubble columns: comparison of detailed experiments and flow simulations, Chem. Eng. Sci. 54 (1999) 5927–5935.
[5] H.A. Jakobsen, B.H. Sannes, S. Grevskott, H.F. Svendsen, Modeling of vertical bubble-driven flows, Ind. Eng. Chem. Res. 36 (1997) 4052–4074.
[6] J.B. Joshi, Computational flow modeling and design of bubble column reactors, Chem. Eng. Sci. 56 (2001) 5893–5933.
[7] A. Sokolichin, G. Eigenberger, A. Lapin, Simulation of buoyancy driven bubbly flow: established simplifications and open questions, AIChE J. 50 (2004) 24–45.
[8] M. Rafique, P. Chen, M. Dudukovic, Computational modelling of gas–liquid flow in bubble columns, Rev. Chem. Eng. 20 (2004) 225–375.
[9] R.F. Mudde, Gravity-driven bubbly flows, Ann. Rev. Fluid. Mech. 37 (2005) 393–423.
[10] D. Pfleger, S. Gomes, N. Gilbert, H. Wagner, Hydrodynamic simulations of laboratory scale bubble columns fundamental studies of Eulerian–Eulerian modelling approach, Chem. Eng. Sci. 54 (1999) 5091–5099.
[11] K. Ekambara, M.T. Dhotre, J.B. Joshi, CFD simulations of bubble column reactors: 1D, 2D and 3D approach, Chem. Eng. Sci. 60 (2005) 6733–6746.
[12] K. Bech, Dynamic simulation of a 2D bubble column, Chem. Eng. Sci. 60 (2005) 5294–5304.
[13] G.N. Glover Cartland, S.C. Generalis, The modeling of buoyancy driven flow in bubble columns, Chem. Eng. Process. 43 (2004) 101–115.
[14] N.G. Deen, T. Solberg, B.H. Hjertager, Large eddy simulation of the gas liquid flow in a square cross-sectioned bubble column, Chem. Eng. Sci. 56 (2001) 6341–6349.
[15] B.N. Vanga Reddy, M.A. Lopez de Bertodano, E. Krepper, A. Zaruba, H.M. Prasser, Two-fluid model LES of a bubble column, in: 11th International topical meeting on Nuclear reactor thermal-hydraulics (NURETH-11), 2005.
[16] M. Milelli, A Numerical Analysis of Confined Turbulent Bubble Plume, Diss. EH. No. 14799, Swiss Federal Institute of Technology, Zurich, 2002.
[17] D. Lakehal, B.L. Smith, M. Milelli, Large eddy simulation of bubbly turbulent shear flows, J Turb. 3 (2002) 1–20.
[18] B. Niceno, B.L. Smith, M.T. Dhotre, Euler–Euler large eddy simulation (EELES) of a square cross-sectional bubble column using the NURESIM CFD platform, in: accepted the 12th International Topical Meeting on Nuclear Reactor Thermal Hydraulics (NURETH-12), Pittsburgh, Pennsylvania, USA, September 30–October 4, 2007.
[19] M. Milelli, B.L. Smith, D. Lakehal, Some new approaches to bubble modeling using CFD. I. Mech Eng Cong & Exp, New York, USA, CD-ROM, 11–16 November, 2001.
[20] J. Smagorinsky, General circulation experiments with the primitive equations, Month. Weather Rev. 91 (1963) 99–165.
[21] M. Germano, U. Piomelli, P. Moin, W.H. Cabot, A dynamic subgrid-scale eddy viscosity model, Phys. Fluids (1991) 31760–31765.
[22] N.G. Deen, B.H. Hjertager, T. Solberg, Comparison of PIV and LDA measurement methods applied to the gas–liquid flow in a bubble column, in: 10th International Symposium on Applications of Laser Techniques to Fluid Mechanics, Lisbon, Portugal, 9–13 July, 2000.

[23] D.A. Drew, Averaged field equations for two-phase media, Stud. Appl. Math. (1971) 133–165.
[24] Y. Sato, M. Sadatomi, K. Sekoguchi, Momentum and heat transfer in two phase bubble flow. Part I theory. Liquid velocity distribution in two phase flow, Int. J. Multiphase Flow 27 (1975) 79167–95177.
[25] Y. Sato, K. Sekoguchi, Liquid velocity distribution in two-phase bubble flow, Int. J. Multiphase Flow 2 (1975) 79–95.
[26] A. Leonard, Energy cascade in large eddy simulations of turbulent fluid flows, Adv. Geophys. 18 (1974) 237.
[27] P. Moin, J. Kim, Numerical investigation of turbulent channel flow, J. Fluid Mech. 118 (1982) 341–377.
[28] W. Jones, M. Wille, Large eddy simulation of a jet in a cross flow, in: 10th Symposium On Turbulent Shear Flows, The Pennsylvania State University, 1995, pp. 41–46.
[29] D.K. Lilly, A proposed modification of the Germano subgrid scale closure method, Phys. Fluids A 4 (1992) 633–635.
[30] O. Simonin, P.L. Viollet, On the computation of turbulent two phase flows in Eulerian Formulation. EUROMECH 234, Toulouse, France, 1988.
[31] R. Clift, K.R. Grace, M.E. Weber, Bubbles, Drops and Particles, Academic Press, New York, USA, 1978.
[32] M. Ishii, N. Zuber, Drag coefficient and relative velocity in bubbly, droplet or particulate flows, AIChE J 5 (1979) 843.
[33] I. Zun, Mechanism of bubble non-homogeneous distribution in two-phase shear flow, Nucl. Eng. Des. 118 (1990) 155–162.
[34] D.A. Drew, R.T. Lahey, The virtual mass and lift force on a sphere in a rotating and straining flow, Int. J. Multiphase Flow 13 (1987) 113–121.
[35] M. Lopez de Bertodano, Turbulent bubbly two phase flow in a triangular duct, PhD thesis, Renselaer Polytechnic Institute, Troy, NY, 1992.
[36] H. Werner, H. Wengle, Large-eddy simulation of flow over and around a cube in a plate channel, in: Durst, et al. (Eds.), Proceedings of the TSF8, Springer, Berlin, 1989, pp. 155–168.
[37] B.L. Smith, M. Milelli, An investigation of confined bubble plumes, in: Presented at the Third International Conference on Multiphase Flow ICMF'98, Lyon, France, 1998.
[38] M. Lance, J. Bataille, Turbulence in the liquid phase of a uniform bubbly air-water flow, J. Fluid Mech. 222 (1991) 95–118.
[39] H. Tennekes, J.L. Lumley, A First Course in Turbulence, MIT Press, Cambridge, MA, USA, 1972.